

Author version: *Hydrol. Sci. J.*, vol.57(4); 2012; 686-704

Simulating the daily discharge of the Mandovi River, west coast of India

K. Suprit¹, D. Shankar², V. Venugopal^{3,4} & N. V. Bhatkar⁵

1 National Institute of Oceanography, CSIR, Dona Paula, Goa 403004, India

Phone: +91-(0)832-2450-312

Fax: +91-(0)832-2450-602

Corresponding Author

suprit@nio.org

2 National Institute of Oceanography, CSIR, Dona Paula, Goa 403004, India

Phone: +91-(0)832-2450-312

Fax: +91-(0)832-2450-602

shankar@nio.org

3 Centre for Atmospheric and Oceanic Sciences,

Indian Institute of Science, Bangalore, Karnataka 560012, India

Phone: +91-(0)80-2293-3073

Fax: +91-(0)80-2360-0865

venu@caos.iisc.ernet.in

4 Divecha Centre for Climate Change

Indian Institute of Science, Bangalore, Karnataka 560012, India

5 National Institute of Oceanography, CSIR, Dona Paula, Goa 403004, India*

Phone: +91-(0)832-2461-184

nagesh_bhatkar@yahoo.com

Received XXXX; accepted XXXX ; open for discussion until XXXX

Citation Suprit, K., Shankar, D., Venugopal, V. & Bhatkar, N. V. (2010) Simulating the daily discharge of the Mandovi River, west coast of India. *Hydrol. Sci. J.* **xx**, xx-xx

* *Present Affiliation: Open Destinations Infotech Pvt Ltd, Campal, Panaji, Goa 403001, India*

Abstract

A hydrological modelling framework was assembled for simulating the daily discharge of the Mandovi River on the Indian west coast. Approximately 90% of the west-coast rainfall, and therefore discharge, occurs during the summer monsoon (June–September), with a peak during July–August. The modelling framework consisted of a digital elevation model (DEM) called GLOBE, a hydrological routing algorithm called THMB (Terrestrial Hydrological Model with Biogeochemistry), an algorithm to map the rainfall recorded by sparse raingauges to the model grid, and a modified Soil Conservation Service Curve Number (SCS-CN) method. A series of discharge simulations (with and without the SCS method) was carried out. The best simulation was obtained after incorporating spatio-temporal variability in the SCS parameters, which was achieved by an objective division of the season into five regimes: the lean season, monsoon onset, peak monsoon, end-monsoon, and post-monsoon. A novel attempt has been made to incorporate objectively the different regimes one encounters before, during, and after the Indian monsoon, into a hydrological modelling framework. The strength of our method lies in the low demand it makes on hydrological data. Apart from information on the average soil type in a region, the entire parameterisation is built on the basis of the rainfall that is used to force the model. That the model does not need to be calibrated separately for each river is important because most of the Indian west-coast basins are ungauged. Hence, even though the model has been validated only for the Mandovi basin, its potential region of application is considerable. In the context of the PUB (Prediction in Ungauged Basins) framework, the potential of the proposed approach is significant because the discharge of these (ungauged) rivers into the eastern Arabian Sea is not small, making them an important element of the local climate system.

Key words hydrological modelling; SCS Curve Number; Sahyadris; river discharge; Mandovi river

1. INTRODUCTION

Orography makes the Indian west coast home to the heaviest rainfall in the Indian subcontinent. The most striking feature of this coast is the presence of the Sahyadris range (upper right inset in Fig. 1), which runs parallel to the coast and therefore lies perpendicular to the summer-monsoon (June–September) winds (Rao, 1976). The dominant mode of precipitation is orographic lifting of the moisture-laden winds blowing from the sea (Sarker, 1966), causing heavy rainfall on the windward side and distinguishing it from the much drier leeward side. The small area and mountainous terrain make it difficult to impound water, leading to a large fraction of the heavy summer-monsoon rainfall flowing into the eastern Arabian Sea through numerous rivers.

Rivers play an important role in the freshwater budget and climate. Although the connection between water resources and rivers is obvious, river discharge is also an important climate variable affecting the regional climate system (Han et al., 2001; Howden and Murtugudde, 2001; Montégut et al., 2007; Shenoi et al., 2002). Recognition of this crucial role played by rivers has led to the assembling of global databases on river discharge (Fekete et al., 2000; Vörösmarty et al., 1996) and the construction of numerical models to simulate river discharge on continental scales (Coe, 2000).

In the Indian subcontinent, however, there is a dearth of information on river discharge (Shankar et al., 2004; SKS04 hereafter). A large number of ungauged rivers along the Indian west coast, and their high runoff (Fekete et al., 2002), makes numerical modelling the only viable tool for predicting the potentially large discharge in these ungauged basins (SKS04; Sivapalan et al., 2003). Therefore, the relevant context for this work is provided by the PUB (Predictions in Ungauged Basins; Sivapalan et al., 2003) programme. It is thus important to be able to simulate the discharge of these rivers, while working within the constraints imposed by the available data, which, for the most part, consists only of a sparse distribution of raingauges.

This need for estimating the freshwater discharge into the seas around India led SKS04 to assemble a quantitative modelling framework. Their framework is based on *Terrestrial Hydrological Model with Biogeochemistry* (THMB), a distributed hydrological model developed by Coe (1998, 2000) (formerly called *HYDrological Routing Algorithm* (HYDRA)). The framework requires only the basic data input for any hydrological model, namely, topography, rainfall, and evapotranspiration. The viability of the framework was demonstrated by SKS04 for the Mandovi (Fig. 1), a typical west-coast river basin.

Since existing rainfall data sets proved inadequate for capturing the large rainfall gradient across the Sahyadris, Suprit and Shankar (2008; SS08 hereafter) developed a method to map the

rainfall using the sparse raingauge data available. To obtain an accurate rainfall distribution, SS08 interpolated the rainfall separately for the windward and leeward sides, and merged the resultant maps using a three-point smoothing. Specifying the ridge was the key to reduce the underestimation (overestimation) of rainfall on the windward (leeward) slopes. The monthly rainfall maps thus generated were used to force THMB. The annual simulated discharge for the Mandovi river basin was within the estimated error of ~15–25% (Coe, 2000; Cogley, 1989; Di Baldassarre and Montanari, 2009; Dickinson, 1967) associated with the observed discharge. Specifically, during 1981–1998, the average error for the discharge simulation was 8% (as compared to the natural variability of 19%).

In the present work, we extend the efforts of SS08 to simulate the daily discharge. The higher temporal resolution demands one major improvement to THMB. SS08 used a constant partitioning of the difference of rainfall and evapotranspiration to obtain the surface and subsurface runoff. This constant partitioning was a good approximation for simulating annual discharge because the annual discharge of the west-coast rivers does not have any memory (SS08): the discharge over a year depends only upon the effective rainfall during that year (Fig. 2). The discharge curve starts from and ends at near zero every year, implying that the discharge of each year is independent of the discharge of the previous year. Hence, details of the discharge curve are not important for simulating the annual discharge and constant parameterisation works. To account for the interannual variability seen in discharge, the framework has to include a more complex rainfall-runoff model than the one used in THMB. It is the development of this rainfall-runoff parameterisation for THMB, given the severe data availability constraints, that is the main contribution of this paper.

We begin by describing the hydrological system being modelled and the existing modelling framework in Section 2. This is followed by the proposed changes to the existing rainfall-runoff model in Section 3. A further modification to account for the spatio-temporal variation of the parameters of the rainfall-runoff model is introduced in Section 4. The strengths and weaknesses of the modelling framework are discussed in Section 5, followed by conclusions in Section 6.

2. DATA AND MODEL

The modelling framework requires rainfall and evapotranspiration data, and a digital elevation model (DEM) to map the topography of the region. Discharge data, where available, are used to validate the simulation results and to build the relevant parameterisations.

The Mandovi is typical of the rivers along the Indian west coast, but it is one of the few that is gauged; it is also one of the best-studied estuaries in India (Shetye et al., 2007). With a length of

87 km and a basin area of 2032 km² (Rao, 1975), it is entirely rain-fed; hence, the discharge is highly seasonal in nature. The discharge gauge on the Mandovi is located at Ganjem (Fig. 1), about 50 km from the mouth (Shetye et al., 1995). The catchment area of Mandovi at the Ganjem is 872 km². The daily discharge data for Ganjem were obtained from the Central Water Commission (CWC), India. Daily rainfall data for 20 stations in and around the Mandovi basin (SS08) were obtained from the India Meteorological Department (IMD).

Most of the rainfall in the Mandovi basin (~ 90%) occurs during the summer monsoon (June–September), with negligible rainfall during December–April (SS08; Shetye et al., 2007). Correspondingly, the daily discharge during December–April is of the order of 0.1 hm³ in contrast to the peak discharge of the order of 100 hm³ observed during the peak summer monsoon (July–August). Depending upon the phase of the monsoon (active or weak/break phase), rainfall, and therefore discharge, peaks show large variability even at the peak of the summer monsoon (Fig. 2). There is also considerable spatial variability in the rainfall in the basin. It increases from west (coastal plain with scattered hills) to east till the Sahyadris range (heavy rainfall on the steep slopes and hills), before collapsing in the rain-shadow region (leeward side) farther eastward. The sparsity of the raingauges — only five raingauges are deployed in the basin — and complex terrain of the basin, make it difficult to map the rainfall variability in space (SS08).

The daily forcing fields of rainfall on the model grid are generated in THMB by interpolating the daily-rainfall data from the 20 raingauges. The interpolation method used is the same as in SS08, but with an important difference. While SS08 merged the maps for the windward and leeward sides using a 3-point smoothing, here we choose to avoid smoothing to permit a sharp decrease in rainfall across the ridge.

A freely available DEM called GLOBE (Global Land One-kilometre Base Elevation) (GLOBE, 2004), with a resolution of 30 arc seconds (~ 1 km) is used to map the topography (Fig. 1) and to derive the basin geometry (SKS04). Owing to its coarse resolution, the GLOBE DEM failed to resolve the narrow river valley in the Mandovi basin. Therefore, SKS04 developed a tool based on GRASS GIS (Neteler and Mitasova, 2002) to edit the DEM manually. The edited DEM resolves the basin geometry accurately and was used by SKS04 and SS08 to simulate the hydrology of the region. SKS04 chose the GLOBE DEM for computational reasons. Our objective is not merely to simulate the discharge of the Mandovi, but to assemble a modelling framework that can be extended to other west-coast rivers. The larger domain involves a much larger number of grid cells, increasing manifold the computational time required for the simulations.

The focus of this work is thus on three aspects of the discharge in the Mandovi. First, we seek an accurate simulation of the observed discharge throughout the rainy period (late May to late October). Second, the large abstraction during the onset phase of the monsoon (late May) is important and the attempt to simulate it leads to much of the parameterisation of the rainfall-runoff model. Third, though the baseflow following the peak monsoon is small, it is almost two orders of magnitude larger than the lean-season flow and is therefore significant enough ($\sim 10 \text{ hm}^3$) to merit accurate simulation.

To build the model parameterisation, or to calibrate the model, we use three of the available 18 years (1981–1998) of rainfall and discharge data. The remaining 15 years are used subsequently to validate the model. The three years (1986, 1990, and 1992) chosen to calibrate the model represent the interannual variability of the data, i.e., low, high, and average rainfall years. These are also three of the six years for which rainfall data are available for all 20 stations (Table III in SS08), thus yielding the best possible spatial rainfall maps. All numerical experiments are carried out for these three years, and only the results of the final numerical experiment are shown for the other 15 years.

2.1 THMB framework

THMB, shorn of the biogeochemistry, is primarily a routing algorithm. A fully distributed grid model, based on the instantaneous unit hydrograph (IUH) formulation, THMB is highly scalable and has been used extensively to simulate water balance for basins of various sizes (Coe 2000; Coe and Foley 2001; Coe et al., 2007, 2009; Donner et al., 2002; Li et al., 2005, 2007; SKS04; SS08). The general formulation of THMB is given in Coe (2000), whereas specific details pertaining to the Mandovi basin are the same as in SKS04 and SS08. Using the GLOBE DEM, the basin is divided into a uniform grid of size $\sim 1 \text{ km} \times 1 \text{ km}$. THMB routes the surface runoff and subsurface runoff through the network of grid cells to its destination, the sea. It uses a linear reservoir model to simulate water transport in terms of local flow directions derived from the local topography, residence times within a grid cell, and effective flow velocities. In each grid cell in this network, the water transport is represented by the time-dependent change of three linear water reservoirs, namely, W_S (surface water reservoir), W_D (subsurface water reservoir), and W_R (river water reservoir) (Fig. 3). The residence times of the water in these reservoirs are T_S , T_D , and T_R , respectively. W_R contains the sum of upstream and local water in excess of that required to fill a local, surface-water depression, W_S contains water that has run off the surface locally and is flowing towards a river, and W_D contains water that has drained through the local soil column and is flowing towards a river. The forcing for

THMB is derived by partitioning the runoff, which is the difference between rainfall (P) and evapotranspiration (E), into surface and subsurface runoff. We have $R_S = \alpha \times (P-E)$ and $R_D = (1-\alpha) \times (P-E)$. The water entering into each cell of the hydrological network is the sum of the surface runoff (R_S), subsurface runoff (R_D), and the flux of water from upstream grid cells ($\sum F_{in}$). The governing equations are the following (Coe, 2000; SKS04; SS08).

$$\frac{dW_S}{dt} = R_S - \frac{W_S}{T_S} \quad (1a)$$

$$\frac{dW_D}{dt} = R_D - \frac{W_D}{T_D} \quad (1b)$$

$$\frac{dW_R}{dt} = \left(\frac{W_S}{T_S} + \frac{W_D}{T_D} \right) - \frac{W_R}{T_R} + \sum F_{in} \quad (1c)$$

Given the surface runoff (R_S) and subsurface runoff (R_D), THMB uses a finite-difference numerical scheme to route the water through the river network to the destination. The direction of flow of R_D is assumed to be the same as that of the R_S , except that the time-scale of R_D is greater than that of R_S . The partitioning of the excess rainfall ($P-E$) was constant in Coe (2000), who used experimental results from large-scale hydrology to set R_S (R_D) to 30% (70%) of the total runoff.

We forced THMB with the daily rainfall maps (obtained using the method of SS08) and analysed the results for the three years 1986, 1992, and 1990; this simulation is called S0 (Fig. 3). The simulated discharge for 1992, along with the observed discharge and the catchment-integrated rainfall, is shown in Fig. 4a. As in SKS04 and SS08, the seasonal cycle is poorly simulated. The cause of this poor simulation is the constant α : the strong seasonal cycle in rainfall and soil moisture, and hence in runoff, in the Mandovi basin implies a time-dependent α .

Constant partitioning of runoff smoothes the observed variability in discharge because this parameterisation ignores the differing hydrological response to variations in space (geographic) and time (climatic). Hence, there is a need for a modified rainfall-runoff parameterisation, which is simple enough to work with the sparsely available data, but capable of accounting for the temporal variability.

3. RAINFALL-RUNOFF PARAMETERISATION

The only observational data available in the Mandovi basin are rainfall and discharge, making the choice of a usable model more difficult. The discharge data are not available for most of the west-coast rivers, ruling out the use of discharge data in model parameterisation. We choose the Soil

Conservation Service Curve Number (SCS-CN; SCS hereafter) method (SCS, 1985), a simple and widely used model, to parameterise the separation of runoff into surface and subsurface runoff.

In the THMB framework, rainfall is mapped onto the grid cells defined by the DEM, and the runoff forcing is generated for each grid cell. In the rest of this section, we incorporate the SCS method into the THMB framework to parameterise the rainfall-runoff relationship.

3.1 Runoff partitioning

We give here a brief but self-contained description of the SCS method, even though it is well known (see Mishra and Singh (2003) for a more detailed description). According to the SCS method, the ratio of the actual runoff to potential runoff is equal to the ratio of the amount of water detained in the basin and the maximum storage in the watershed. Thus, R_S and R_D , the surface and subsurface runoff in THMB, are defined as follows in the SCS formulation:

$$P = R_S + I_a + F_a \quad (2a) \quad R_D = b \times F_a \quad (2d)$$

$$\frac{F_a}{S} = \frac{R_S}{P - I_a} \quad \text{for } P > I_a \quad (2b) \quad R_D = P - R_S - I_a \quad (2e)$$

$$R_S = \frac{(P - I_a)^2}{(P - I_a + S)} \quad (2c) \quad I_a = \lambda \times S \quad (2f)$$

$$S = \frac{25400}{CN} - 254 \quad (2g)$$

where P is the rainfall, I_a the initial abstraction (amount of rainfall for which there is no runoff), F_a the water detained in the basin, and S the storage in the basin. All the above quantities are in mm. The base flow index, b , varies between 0 and 1. Equations (2f) and (2g) involve non-dimensional parameters, λ (initial abstraction coefficient) and CN (Curve Number). Except R_S , R_D , and b , all the notations here have the standard meaning as in the SCS method.

As data on infiltration are meagre, estimation of R_D is difficult. Hence, as in Geetha et al. (2007), we use equations (2d) and (2e) to define R_D . Since baseflow is small in the Mandovi basin, we assume that all the water that infiltrates contributes to R_D , i.e., $b=1$. Hence, as in the original THMB formulation, there is no groundwater-recharge term in the model and the only loss term is I_a (equivalent to evapotranspiration in THMB).

λ depends on the geographic and climatic conditions of the watershed (Ponce and Hawkins, 1996; Mishra and Singh, 2003) and a wide range of λ (0–1) has been reported in the hydrology literature. A practical range for CN, which depends on the physical properties of the watershed (soil

type, vegetation cover, etc.), is 40–100 (Mishra and Singh, 2003). For the Mandovi, we pick 60–90 as the possible range of CN for our study.

The CN used in equation (2g) represents an average or normal hydrological condition in the basin, i.e., it does not account for the antecedent moisture conditions, whose variability translates into variability of the basin’s runoff generation potential. This variability is incorporated by a simple parameterisation scheme called AMC (Antecedent Moisture Conditions) to differentiate dry and wet soil conditions from the average soil condition (Chow et al., 1988; Mishra and Singh, 2003). The CN(I) (dry) and CN(III) (wet) are calculated from the average CN (CN(II)) by the empirical expressions given below (Chow et al., 1988):

$$CN(I) = 4.2 \times \frac{CN(II)}{10 - 0.048CN(II)} \quad (3a)$$

$$CN(III) = 23 \times \frac{CN(II)}{10 + 0.13CN(II)} \quad (3b)$$

Application of the above parameterisation (with the conventional five-day AMC threshold) to the Mandovi basin demands a sensitivity test to determine the optimum values of the SCS parameters: CN, λ , and the AMC thresholds.

3.2 Sensitivity to SCS parameters

For the CN range 60–90, we carried out simulations to test the sensitivity of the simulated discharge to CN (Fig. 5a). In all these experiments, the initial abstraction coefficient λ was set to 0.2 (SCS-recommended), and the lower and upper AMC thresholds were 100 and 250 mm. Five-day antecedent rainfall less (greater) than 100 (250) mm is equivalent to dry (wet) AMC and correspondingly CN(I) (CN(III)) is used. The correlation between the simulated and observed discharge was comparable across this CN range, but was highest for CN equals to 80. The results were similar to S0: higher (lower) CN values resulted in higher (lower) simulated discharge irrespective of seasonality.

The range of CN values for the above experiments was based on the different soil and hydrological characteristics in the basin. In spite of its small size, the Mandovi basin shows a great degree of variability in these characteristics. On one hand, the regime of the Sahyadris, with steep slopes and hard soils, implies large CN values; on the other hand, the coastal sandy area implies low CN. Hence, a representative value of CN for the entire basin is 70.

Simulations were also done for different values of λ , the abstraction coefficient: 0.05, 0.2, 0.3, and 0.6. For all these simulations, CN was fixed at 70 for the entire basin and the AMC thresholds

were also fixed as in the CN sensitivity tests. The results (Fig. 5b) show that the simulated discharge is not as sensitive to λ as it is to CN. Note that in these sensitivity tests (Fig. 5b), λ was varied by over 100% in comparison to the $\sim 10\%$ variation in the CN sensitivity tests.

We selected 100 and 250 mm as the appropriate lower threshold (distinguishing the dry and average AMC) and upper threshold (distinguishing the average and wet AMC), respectively. These values are significantly larger than those initially recommended by SCS (SCS, 1985). Subsequently, however, SCS recognised that these AMC thresholds would not be valid for different geographical and climatic regimes, and therefore discontinued prescribing the SCS thresholds in its subsequent publications. The recommendation is that the AMC thresholds should be chosen based on the conditions in the study region (Ponce and Hawkins, 1996). Accordingly, these thresholds were chosen such that $1/e$ ($\sim 36\%$) of the days had rainfall above the lower threshold and $1/e^2$ ($\sim 14\%$) of the days had rainfall over the upper threshold; $\sim 22\%$ of the days experienced “average” rainfall (Fig. 6). The hydrological rationale for these numbers is as follows. The soil and land are expected to adjust to the normal or expected runoff over most of the rainy season. Hence, we assume that the dry CN, implying greater storage and lower runoff, would hold for $(1-1/e)$ of the days and that the average CN would hold for $(1-1/e)$ of the remaining $1/e$ days, leaving $1/e^2$ of the days in the higher-than-average-rainfall band. The simulations also suggest that this argument is reasonable.

3.3 Results

We use $CN=70$, $\lambda=0.2$, and AMC thresholds of 100 and 250 mm as the optimum basin-average values. This simulation, called S1, uses the SCS prescribed parameters, and yielded a much higher correlation than did S0, and there were two major improvements (Fig. 4b). First, as expected, the baseflow decreased to more realistic levels during the weak spells of the peak-monsoon season (July–August). Second, as with the observed discharge, there was greater variability in the simulated discharge in S1 than in S0. The reason for these improvements is that the high CN values in the average and wet periods lead to a dominance of surface runoff at these times and the relatively low CN during the dry periods allows much of the rainfall to be abstracted.

One drawback of S1 is the underestimation of the discharge following the peak of the monsoon, i.e., the simulated baseflow in September is lower than observed. The main issue, however, is the overestimation of the discharge during the onset phase of the monsoon (May–June; Fig. 4b). One possible reason is an overestimation of the runoff on the lee side, which is drier than the windward side and should therefore have lower CN values compared to the slopes of the Sahyadris. The SCS parameters in S1 were, however, constant across the basin and did not account

for such spatial differences. Another possible reason is that the onset-phase CN is overestimated on the windward side too. The basin is much drier before the monsoon than after onset, and the storage capacity should therefore vary accordingly. The SCS parameters in S1 did not, however, vary with season, leading to a possible overestimation of the onset-phase surface runoff. The sensitivity of the simulations to the SCS parameters implies a large potential variation in the rainfall-runoff relationship across the basin, and possibly also in time. In other words, the five-day AMC used in S1 is not sufficient to capture the spatial and temporal variations that are likely in the SCS parameters even within this small basin. The challenge is to incorporate these variations in a manner that is not only physically reasonable, but also simple. Nevertheless, incorporating the SCS method into THMB does improve the simulated discharge, suggesting that this simple parameterisation is useful.

4. SPATIO-TEMPORAL VARIABILITY OF THE SCS PARAMETERS

4.1 Spatial variability

Ideally, estimating the SCS parameters requires rainfall and runoff data from the catchment area, or, in the case of a distributed model like THMB, from each grid cell. The reason for spatial variation in the SCS parameters (CN, λ and AMC thresholds) is the spatial variation in soil type, vegetation cover, land use, and hydrological and moisture conditions. Though the rainfall-mapping procedure provides rainfall information for each grid cell, we do not have runoff information for the cells. The only information available on runoff is the discharge at Ganjem.

Hence, we use the elevation to divide the basin into four hydrological regions (lower right inset in Fig. 1): the leeward side of the Sahyadris (Lee), the ridge and the windward slope above 200 m (Ridge), the foothills of the Sahyadris or the region on the windward side between elevation contours 40 and 200 m (Foothills), and the coastal plains or the region at an elevation below 40 m (Coast). The SCS parameters were determined for each of these regions.

The CN was estimated on the basis of the runoff-generation capacity of the soil in the region because detailed information on soil cover was not available. The dominant soil type and land usage for the four regions are listed in Table 1. From the soil type listed in Table 1, it is evident that the Ridge region has the maximum runoff-generation capacity, followed by Foothills, Lee, and Coast. λ was estimated similarly and AMC thresholds were determined the same way as done earlier (Section 3.2).

4.2 Temporal variability

The excess rainfall in the Mandovi basin appears neither as streamflow (immediately following the rain) nor as baseflow (appearing after a lag) (Figs. 2 and 4). This excess rainfall must therefore either recharge the groundwater or be returned to the atmosphere through evapotranspiration. On the catchment scale, groundwater recharge is a small quantity (Coe, 2000; Maréchal et al., 2009) and has been neglected in the THMB formulation. Evapotranspiration is therefore the only loss term in this model, and in the absence of observations (Maréchal et al., 2009), it is implicitly parameterised in the SCS method using the initial abstraction, which is a function of CN and λ .

Before the onset of monsoon, the soil is dry, temperature is high, and relative humidity is low. Transpiration through the vegetation canopy also leads to a loss of water from the basin (Maréchal et al., 2009). Therefore, there exists a large potential for initial water retention and evapotranspiration whenever moisture becomes available.

The basin characteristics change dramatically once the monsoon sets in. The soil begins to soak up moisture, temperature decreases, and relative humidity increases. Evapotranspiration is highest during this transition period. It is higher than during the preceding dry season because the actual evapotranspiration is limited by the amount of water available. Hence, abstraction is at its peak during the onset phase. Not accounting for this high abstraction leads to an overestimate of the discharge at this time (Fig. 4b).

Immediately after the monsoon peaks, the soil is still saturated. Hence, the runoff responds rapidly to rainfall (Fig. 2) and the abstraction remains low. Later, the soil dries out, but the availability of water becomes the limiting factor, and abstraction remains low till the following year's onset.

Thus, the SCS parameters exhibit an inherent seasonality, which cannot be accounted for by the conventional five-day AMC parameterisation. The rest of our work attempts to incorporate the temporal variation of the SCS parameters into the rainfall-runoff model.

4.3 Seasonal variation of SCS parameters

In order to build a time-dependent parameterisation of the SCS parameters, we need to distinguish the different rainfall-runoff regimes during the season, and define objective criteria for transition from one regime to another. We use daily rainfall and discharge (the only available data) to describe these temporal regimes, but use only rainfall and its accumulation over time as the criteria for transition from one regime to another.

The temporal regimes are described in Table 2 and depicted graphically in Fig. 7. Five distinct temporal regimes are identified in the Mandovi basin. The first regime is the Lean-Season Regime (A) at the beginning and end of a calendar year. This regime is very dry and the discharge is primarily baseflow. The transition (called AB) to the Monsoon-Onset Regime (B) is marked by the first spells of rain. Regime B is wet; however, since the soil is still unsaturated, the discharge does not respond to rainfall. The transition (BC) to the Peak-Monsoon Regime (C) is marked by a big rainfall burst and a sharp inflection of the cumulative-rainfall (CR) curve (Fig. 7). The soil is saturated by now, and the basin responds to rainfall in the form of instantaneous pooling. Rainfall is more sustained during this transition and lasts a few days, leading to a different slope for the CR curve during this regime in comparison to the onset regime (B). The transition (CD) to the End-Monsoon Regime (D) is marked by a break in rainfall. There is little or no rainfall for five or more days, the CR curve plateaus off (marking a second major inflection point; Fig. 7), and the discharge recedes exponentially. During Regime D, there are some rainfall bursts (weaker than those during Regime C), and the discharge still responds to these bursts because the soil is wet and saturated. The transition (DE) to the Post-Monsoon Regime (E) is marked by a longer rainfall break, which lasts for 10–15 days. During this regime, the soil is moist (but unsaturated), and the discharge stops responding to the weak and scattered rainfall. The last transition (EA) occurs towards the end of the year and is marked by a longer (~30 days) rainfall break.

Objective criteria for transition

The transitions described above need quantification, i.e., a set of objective criteria are needed to determine the period of transition. The criteria we use (Table 3) are applied to each grid cell of the Mandovi River basin.

The first transition to be determined is AB, i.e., the onset date (phase) of the monsoon. The rainfall condition for AB transition (Column 2, Table 3) is similar to that used by IMD to determine the date of onset of the monsoon over Kerala (Ananthkrishnan et al., 1968; Pai and Nair, 2009). A more complex criterion recently adopted by IMD results in a similar date for monsoon onset (Pai and Nair, 2009). The second transition, BC, is marked by a sharp increase in rainfall and a corresponding sharp, concave-upward inflection in the CR curve (Fig. 7), which we capture by noting the deviation of the curve from a line fitted to the CR curve over Regime B (column 3 and CR1 in Table 3). The third transition, CD, is opposite to BC (column 4 and CR2 in Table 3). The CR curve plateaus off, resulting in another sharp inflection, but now in the opposite direction, i.e., the inflection is concave-down (Fig. 7). Once Regime D sets in, the CR curve is too flat for it to be used as a criterion to

determine Transition DE (Fig. 7). Hence, criteria based on AMC and rainfall are used to determine DE (column 5, Table 3). The transition to the lean-period regime, EA, is deemed to occur if the daily rainfall is equal to or less than the trace rainfall (1 mm) for 30 consecutive days (column 6, Table 3).

The SCS parameters have to be estimated for each regime for each of the four regions. We used the “mean conditions” to define the average basin CN(II) and used this CN(II) to estimate the dry-period and wet-period CN(II). The average conditions are represented for the Mandovi by Regime E, the post-monsoon season, when the soil is still moist but unsaturated. CN values chosen for each region for each of the five regimes discussed are listed in Table 4. Regime C is an extreme case and almost all the rainfall is converted to surface runoff because the soil is completely saturated. Hence, for this regime, we set the CN(II) for all four regions to 90. Empirical estimates of CN(II) for Indian watersheds spanning a range of hydrological regimes suggest that a high value is appropriate during rainfall events (Mishra et al., 2008). The CN(II) values we use are comparable to, but less than, those reported by Mishra et al. (2008) because their estimates were based on very few events.

Just as the CN shows considerable variation with season, so must λ and AMC thresholds. The AMC thresholds were determined the same way as done earlier (Section 3.2). The exceptions to this rule were Regimes B and C, where different exponential cut-offs were used to reflect the higher number of dry days in Regime B and the mostly wet conditions in Regime C. λ and AMC thresholds are listed in Table 4.

4.4 Results and Validation

Simulation S2 was made using the spatio-temporally varying parameters listed in Table 4. Simulations incorporating only spatial variability showed no improvement over S1. The results of S2 (Fig. 4c) show a significant improvement over S1. The simulated discharge matches the observed discharge better across a range of conditions. Specifically, the simulated discharge increases during the rainfall bursts in July, August, and September, resulting in a better match with observations. The increase in discharge, however, is also seen during the weak spells in early July, when S2 performs worse than S1. The sharp increase in CN with Transition BC increases the discharge even during the weak spells. The results for the other two years, 1986 and 1990, are similar.

We built the model parameterisation using data for only three (1986, 1990, and 1992) of the 18 years; validation of the model is done using the remaining 15 years. The results of S2 for four of the other 15 years are shown in Fig. 8; these four years include two years (1981, 1991) for which rainfall data are available for all 20 stations and two years (1987, 1994) for which rainfall data are missing for some stations (SS08). The results for other years are similar. The model parameterisation

works as well for the entire data set as it does for the three calibration years: correlations for 15 years of data are 0.67 (S0), 0.76 (S1), and 0.80 (S2). The major improvement in S2 is the lack of underestimation of discharge (Fig. 9). Though S2 has a greater tendency to overestimate the discharge during June–August, there is an overall improvement. S2 captures better the variability over the range of temporal hydrological regimes (Fig. 4c and Fig. 8). Indeed, the strength of S2 lies in its ability to simulate the discharge better across the spectrum of variability from the seasonal to the interannual (Fig. 9). The simpler five-day AMC parameterisation fails to account for this spectrum of variability not only over a season, but also across years.

We find that there is a tendency to overestimate the discharge at some times in some years. This is particularly evident when there is a long dry period during the peak monsoon (1992, 1998; figure not shown), and the soil probably becomes unsaturated, or, when the peak-monsoon regime sets in early (e.g., 1990). Other than these discrepancies, the model performance is remarkable, and the simulated discharge matches well with the observed discharge across all the regimes.

5. DISCUSSION

A modelling framework has been assembled for simulating the daily discharge of a poorly gauged Indian west-coast river. The strength of the proposed framework lies in the incorporation of the SCS method, modified to allow spatio-temporal variability of the SCS parameters, into THMB. Specifically, we have objectively incorporated the various kinds of regimes one encounters before, during and after the Indian monsoon, into a hydrological modelling framework. Incorporating this spatial and temporal variability in the model parameterisation improved the daily discharge simulation substantially. The strength of the proposed modelling framework lies in its low demand on the input data, which is particularly important for an ungauged basin. Apart from information on the soil type in the basin, the entire model parameterisation is built using only the forcing, i.e., rainfall. All model parameters are derived on the basis of rainfall, which is a basic requirement for any hydrological model.

Though the comparison between simulated and observed discharge is good, there is scope for improving the parameterisation. One notable drawback is the need to specify a minimum duration of 60 days for the peak-monsoon regime. This specification was necessitated by the need to preclude a prolonged weak spell or break triggering a transition to the post-monsoon regime. Another caveat is the specification of absolute rainfall thresholds as one of the criteria for Transition BC. Absolute thresholds are prone to giving erroneous results when the rainfall is “not normal”. A more serious caveat is the averaging of AMC thresholds across a region. Ideally, the thresholds ought to be

allowed to vary across the region to account for spatial heterogeneity of rainfall.

We have also examined the applicability of the modelling framework to other west coast rivers. We expect the framework to work for all west-coast rivers that have geographical and climatic regimes similar to the Mandovi. A plot of the observed discharge for some rivers on the west coast (Fig. 10) indicates that the discharge patterns are comparable across most of the coast: the inter-river variability is no more than the interannual variability for any river, suggesting that the model with the proposed modifications should work for these basins as well.

It was this need to extend the framework to other west-coast rivers that led SKS04 to choose the GLOBE DEM, whose resolution of 30 arc seconds is fairly coarse for a small basin like the Mandovi. Hence, since the computational power available has increased manifold since SKS04 chose GLOBE, we have run some preliminary simulations with the SRTM DEM (Farr et al., 2007). We find that even such high-resolution DEMs need editing for flow routing. Hence, given the much larger number of grid cells, their use will require integration of automatic terrain analysis algorithms (e.g., *ANUDEM* (Hutchinson, 1989), *PEM4PIT* (Grimaldi et al., 2007), and *Terraflow* (Toma et al., 2003)) into the modelling framework, alleviating the need for manual editing. Incorporation of high-resolution DEMs in this modelling framework for future applications will be a natural extension of this work.

6. CONCLUSIONS

A novel hydrological modelling framework has been assembled to successfully simulate the daily discharge of a poorly-gauged river, Mandovi, along the west-coast of India. The novelty of the proposed framework is two-fold: (i) Incorporation of the SCS-CN rainfall-runoff model into THMB, which is essentially a routing algorithm; and (ii) Modification of the SCS-CN method to incorporate spatial and temporal variations in the parameters: CN, λ , and the AMC thresholds. Furthermore, the criteria used to determine the temporal variation of the SCS-CN parameters are based only on rainfall, the main forcing for the model. This dependence of the parameterisation on just the rainfall is one of its chief merits.

Preliminary analysis of the discharge of other west-coast rivers indicate that the proposed framework should work for other basins as well. That the model does not need to be calibrated separately for each river is of paramount importance because most of these basins are ungauged. Hence, even though the model has been validated here only for the Mandovi, its potential region of application is considerable and spans most of the Indian west coast. In the context of PUB, the potential of the proposed framework is significant because the discharge of these (ungauged) rivers

into the eastern Arabian Sea is not small , hence making them an important element of the local climate system.

Acknowledgements This work was supported by grants from CSIR (Council for Scientific and Industrial Research), New Delhi. K. Suprit acknowledges the financial support from CSIR and National Institute of Oceanography, Goa. IMD and CWC provided the rainfall and river-discharge data. S.R. Shetye inspired and encouraged us to take up this work. We acknowledge the helpful discussions we had with D. Nagesh Kumar. M.T. Coe made available the original THMB code and H. Mitasova's RST method was used for rainfall interpolation. We acknowledge the role of GRASS GIS in this study and thank the GRASS team. The RST code was integrated with THMB with help from Soumava Ghosh and Mandeep Singh. Ferret and GMT were used extensively for analysis and graphics. We are grateful to the two anonymous reviewers for their constructive comments and suggestions. This is NIO contribution XXXX.

REFERENCES

1. Ananthkrishnan, R., Srinivasan, V., Ramakrishnan, A. R. & Jambunathan, R. (1968) Synoptic features associated with onset of southwest monsoon over Kerala. *Forecasting Manual*, FMU Rep. IV-18.2, India Meteorological Department, Pune.
2. Chow, V. T., Maidment, D. R. & Mays, L. W. (1988) *Applied Hydrology*. Water resources and Environmental Engineering, McGraw-Hill Book Company, Singapore.
3. Coe, M. T. (1998) A linked global model of terrestrial hydrologic processes: simulation of modern rivers, lakes, and wetlands. *J. Geophys. Res.* **103**, 8885–8899.
4. Coe, M. T. (2000) Modeling terrestrial hydrological systems at the continent scale: Testing the accuracy of an atmospheric GCM. *J. Clim.* **13**, 686–704.
5. Coe, M. T. & Foley, J. A. (2001) Human and natural impacts on the water resources of the Lake Chad basin. *J. Geophys. Res.* **106**, 3349–3356
6. Coe, M. T., Costa, M. H. & Howard, E. A. (2007) Simulating the surface waters of the Amazon River Basin: impacts of new river geomorphic and dynamic flow parameterizations. *Hydrol. Process.* **21**, 12
7. Coe, M. T., Costa, M. H. & Soares-Filho, B. S. (2009) The influence of historical and potential future deforestation on the stream flow of the Amazon River - Land surface processes and atmospheric feedbacks. *J. Hydrol.* **369**, 165–174
8. Cogley, J. G. (1989) Run-off from the world's landmasses: Amounts and uncertainties at 2-degree resolution. *Trent Climate Note* **89**(3), 25.
9. Di Baldassarre, G. & Montanari, A. (2009) Uncertainty in river discharge observations: A quantitative analysis. *Hydrol. Earth System Sci.* **13**, 913-921.

10. Dickinson, W.T. (1967) Accuracy of discharge determinations. *Hydrology Paper 20*, Colorado State University, Fort Collins, USA.
11. Donner, S. D., Coe, M. T., Lenters, J. D., Twine, T. E. & Foley, J. A. (2002) Modeling the impact of hydrological changes on nitrate transport in the Mississippi River Basin from 1955–1994. *Global Biogeochem. Cycles*. **16**, doi:10.1029/2001GB001396.
12. Farr, T. G., Rosen, P. A., Caro, E., Crippen, R., Duren, R., Hensley S., Kobrick, M., Paller, M., Rodriguez, E., Roth, L., Seal, D., Shaffer, S., Shimada, J., Umland, J., Werner, M., Oskin, M., Burbank, D. & Alsdorf, D. (2007), The Shuttle Radar Topography Mission, *Rev. Geophys.*, **45**, doi:10.1029/2005RG000183.
13. Fekete, B., Vörösmarty, C. & Grabs, W. (2000) Global composite runoff fields on observed river discharge and simulated water balances. *Report 22*. Global Runoff Data Center, Federal Institute of Hydrology (BfG), Koblenz.
14. Fekete, B., Vörösmarty, C. & Grabs, W. (2002) High resolution fields of global runoff combining observed river discharge and simulated water balances. *Global Biogeochem. Cycles* **16**, doi: 10.1029/1999GB001254.3.
15. Geetha, K., Mishra, S. K., Eldho, T. I., Rastogi, A. K. & Pandey, R. P. (2007) Modifications to SCS-CN method for long-term hydrologic simulation. *J. Irrigat. Drain. Eng.* **133**, 475–486.
16. GLOBE (2004) The Global Land One kilometre Base Elevation (GLOBE) Digital Elevation Model. Version 1.0. National Oceanic and Atmospheric Administration, National Geophysical Data Center, <http://www.ngdc.noaa.gov/mgg/topo/globe.html>
17. Grimaldi, S., Nardi, F., Di Benedetto, F., Istanbuloglu, E. & Bras R. L. (2007) A physically-based method for removing pits in digital elevation models, *Adv. Water Resour.* **30**, 2151–2158.
18. Han, W., McCreary, J. P. & Kohler, K. E. (2001) Influence of precipitation minus evaporation and Bay of Bengal rivers on dynamics, thermodynamics, and mixed layer physics in the upper Indian Ocean. *J. Geophys. Res.* **106**, 6895–6916.
19. Howden, S. D. & Murtugudde, R. (2001) Effect of river inputs into the Bay of Bengal. *J. of Geophys. Res.* **106**, 19825–19843.
20. Hutchinson, M. F., (1989) A new procedure for gridding elevation and stream line data with automatic removal of spurious pits, *J. Hydrol.* **106**, 211–232, DOI: 10.1016/0022-1694(89)90073-5.
21. Li, K. Y., Coe, M. T. & Ramankutty, N. (2005) Investigation of hydrological variability in West Africa using land surface models. *J. Clim.* **18**, 3173–3188
22. Li, K.Y., Coe, M.T., Ramankutty, N. & De Jong, R. (2007) Modeling the hydrological impact of land-use change in West Africa. *J. Hydrol.* **337**, 258–268
23. Maréchal, J. C., Varma, M. R. R., Riotte, J., Vouillamoz, J. M., Mohan Kumar, M. S., Rui, L., Sekhar, M. & Braun, J. J. (2009) Indirect and direct recharges in a tropical forested watershed: Mule Hole, India. *J. Hydrol.* **364**, 272–284.

24. Mishra, S. K., Pandey, R. P., Jain, M. K. & Singh, V. P. (2008) A rain duration and modified AMC dependent SCS-CN procedure for long duration rainfall-runoff events. *Water Resour. Manag.* **22**, 861–876.
25. Mishra, S. K. & Singh, V. P. (2003) *Soil conservation Service Curve Number (SCS-CN) Methodology*. Volume 42 of Water Science and Technology Library, Kluwer Academic Publishers, Dordrecht, Netherlands.
26. Montégut, C. d.B., Vialard, J., Shenoi, S. S. C., Shankar, D., Durand, F., Ethé, C. & Madec, G. (2007) Simulated seasonal and interannual variability of the mixed layer heat budget in the Northern Indian Ocean. *J. Clim.* **20**, 3249–3268.
27. Neteler, M. & Mitasova, H. (2002) *Open Source GIS: A GRASS GIS Approach*. Kluwer Academic Publishers: Dordrecht.
28. Pai, D. S. & Nair, M. R. (2009) Summer monsoon onset over Kerala: New definition and prediction. *J. Earth Syst. Sci.* **118**, 123–135.
29. Ponce, V. M. & Hawkins, R. H. (1996) Runoff curve number: Has it reached maturity? *J. Hydrolog. Eng.* **1**, 11–19.
30. Rao, K. L. (1975) *India's Water Wealth: Its Assessment, Uses and Projections*. Orient Longman, New Delhi.
31. Rao, Y. P. (1976) Southwest monsoon. *Meteorological monograph*, India Meteorological Department, New Delhi, India.
32. Sarker, R. P. (1966) A dynamical model of orographic rainfall. *Mon. Weather Rev.* **94**, 555–572.
33. SCS (1985) *National Engineering Handbook, Section 4: Hydrology*, Soil Conservation Service, United States Department of Agriculture, Washington DC.
34. Shankar, D., Kotamraju, V. & Shetye, S. R. (2004) A quantitative framework for estimating water resources in India. *Curr. Sci.* **86**, 543–552.
35. Shenoi, S. S. C., Shankar, D. & Shetye, S. R. (2002) Differences in heat budgets of the near-surface Arabian Sea and Bay of Bengal: Implications for the summer monsoon. *J. Geophys. Res.* **107**, doi: 10.1029/2000JC000679.
36. Shetye, S. R., Gouveia, A. D., Singbal, S. Y., Naik, C. G., Sundar, D., Michael, G. S. & Nampoothiri, G. (1995) Propagation of tides in the Mandovi–Zuari estuarine network. *Proc. Indian Acad. Sci. Earth Planet. Sc.* **104**, 667–682.
37. Shetye, S. R., Shankar, D., Neetu, S., Suprit, K., Michael, G. S. & Chandramohan, P. (2007) The environment that conditions the Mandovi and Zuari estuaries. In: *The Mandovi and Zuari Estuaries* (Eds.) S. R. Shetye, M. Dileep Kumar, and D. Shankar, National Institute of Oceanography, Goa.
38. Sivapalan, M., Takeuchi, K., Franks, S. W., Gupta, V. K., Karambiri, H., Lakshmi, V., Liang, X., McDonnell, J. J., Mendiondo, E. M., O'Connell, P. E., Oki, T., Pomeroy, J. W., Schertzer, D., Uhlenbrook, S. & Zehe, E. (2003) IAHS decade on Predictions in

Ungauged Basins (PUB), 2003–2012: Shaping an exciting future for the hydrological sciences. *Hydrol. Sci. J.* **48**, 857–880.

39. Suprit, K. & Shankar, D. (2008) Resolving orographic rainfall on the Indian west coast. *Int. J. Climatol.* **28**, 643–657.
40. Toma, L., Wickremesinghe, R., Arge, L., Chase, J. S., Vitter, J. S., Halpin, P. N., & Urban, D. (2003) Flow computation on massive grid terrains. *GeoInformatica, Int. J. Adv. Comput. Sc. Geog. Inf. Syst.*, **7**, 283–313.
41. Vörösmarty, C. J., Fekete, B. M. & Tucker, B. A. (1996) Global river discharge database (RivDis Version 1.0), *Vol. 0: Introduction, overview, and technical notes*. International Hydrological Program, technical document in hydrology SC. 96/WS/26. UNESCO, Division of Water Sciences, 1 rue Miollis, 75732 Paris, France.

List of Tables

Table 1 Basin soil and hydrological characteristics and base SCS parameters for the four hydrological regions. The AMC thresholds for each of the four regions were determined on the basis of a histogram of rainfall during May–October and a cumulative frequency curve of the five-day rainfall.

Parameter	Lee	Ridge	Foothills	Coast	Remarks
Soil type	Red, laterite	Shallow soils overlying impervious material (rock)	Red, sandy loam	Sandy soil	—
Land use	Mixed, Forest	Forest	Mixed	Mixed	—
Hydrological soil group	B/C	D	C	A	A (lowest runoff) and D (highest runoff)
CN(II)	65	75	70	60	—
AMC thresholds (mm)	Dry < 100	< 150	< 100	< 100	Based on five-day antecedent rainfall
	Wet > 200	> 400	> 250	> 200	
Initial abstraction coefficient (λ)	0.3	0.05	0.1	0.3	SCS recommended value is 0.2

Table 2 Classification of the hydrological regimes (temporal; Fig. 7) and of the transitions from one regime to the next.

Classification	Physical Condition	Rain	Cumulative rain (CR)	Discharge
A Lean Season	Very dry	No or scanty rainfall	Very small	No discharge
Transition AB		First spells of rain	Small inflection	—
B Monsoon-Onset	Wet (Unsaturated)	Either a break-active cycle or continuous rain peaks	Rising	No response to rainfall
Transition BC		A bigger burst that continues into the peak of the monsoon (3–6 days into the burst)	First large inflection (upslope)	Starts responding to rainfall
C Peak-Monsoon	Very wet	Intense and continuous	Rising rapidly over a sustained period (with plateaus during weak spells)	Follows the rainfall curve
Transition CD		Rainfall break (little or no rainfall) for 5 or more days	Second large inflection (downslope)	Receding exponentially
D End-Monsoon	Wet, Saturated	Active period at the end of the monsoon (late-monsoon rainfall bursts)	Flattening with a few fluctuations	Still responds to some bigger rain bursts
Transition DE		Longer break of 10–15 days		Smooth decline continues
E Post-Monsoon	Moist (Unsaturated)	Smaller scattered bursts of rainfall	Plateau	Stops responding to the rain
Transition EA		30 days of no rainfall	Maximum	—
A Lean Season	Very Dry	No or scanty rainfall	Maximum	No discharge

Table 3 Objective criteria for transition from one regime to the next. Note that CR is estimated starting from the beginning of a year.

	AB	BC	CD	DE	EA
CR	≥ 75 mm	see CR1 below	see CR2 below	—	—
AMC	—	—	—	AMC ≤ 30 mm for 5 consecutive days	
Rain	(1) 3-day rainfall sum ≥ 30 mm (2) Rain ≥ 5 mm on each of these 3 days	Rain ≥ 150 mm	Rain ≤ 5 mm for one day	Rain ≤ 5 mm for 15 consecutive days	Rain ≤ 1 mm for 30 consecutive days
Remarks	Both conditions have to be satisfied.	(1) If the rain condition is satisfied, transition occurs after five days. (2) If not, CR1 condition has to be satisfied. (3) Transition occurs if one of the two conditions is met.	The CR2 condition has to be satisfied first and the rainfall condition is applied afterwards.	(1) The AMC condition has to be satisfied first, and the rainfall condition follows it. (2) The AMC condition is applied only once. If the rain condition fails the first time, it is applied till it is satisfied.	This transition occurs in December.
CR1	Fit a straight line to the CR data and compare the deviation of the curve from the line. Transition occurs if the deviation (concave-up inflection) exceeds one and half standard deviation for five consecutive days				
CR2	Fit a straight line to the CR data and compare the deviation of the curve from the line. Transition occurs if the deviation (concave-down) exceeds one and half standard deviation for five consecutive days				

Table 4 SCS parameters for Simulation S2 (spatial and temporal variation). The numbers in parentheses in the first column represent the parameter choices for Simulation S1; these parameters are used for Regime E. The CN(II) for Regime B is computed using Equation (3a) (dry AMC) and the CN(II) for Regime E. The CN(II) for Regime D is computed using Equation (3b) (wet AMC) and the CN(II) for Regime E. Regime E therefore represents the average or central hydrological regime, Regimes B and D the dry and wet regimes, and Regimes A and C the extremely dry and wet regimes.

	Lean period (A)	Onset Monsoon (B)	Peak Monsoon (C)	End Monsoon (D)	Post Monsoon (E)
	Very dry	Wet (Unsaturated)	Very wet	Wet (Saturated)	Moist (Unsaturated)
Region	CN				
Lee (65)	40	44	90	81	65
Ridge (75)	40	56	90	87	75
Foothills (70)	40	49	90	84	70
Coast (60)	40	40	90	78	60
Region	Initial abstraction coefficient (λ)				
Lee (0.3)	0.3	0.2	0.05	0.2	0.3
Ridge (0.05)	0.3	0.2	0.05	0.05	0.2
Foothills (0.1)	0.3	0.2	0.05	0.05	0.2
Coast (0.3)	0.3	0.2	0.05	0.2	0.3
Region	AMC (five-day antecedent rainfall range in mm)				
Lee (100–200)	30–40	200–250	50–100	20–40	5–20
Ridge (150–400)	40–70	300–450	100–200	30–60	5–20
Foothills (100–250)	50–70	350–450	50–100	20–50	5–20
Coast (100–200)	50–60	400–450	50–100	20–50	5–20

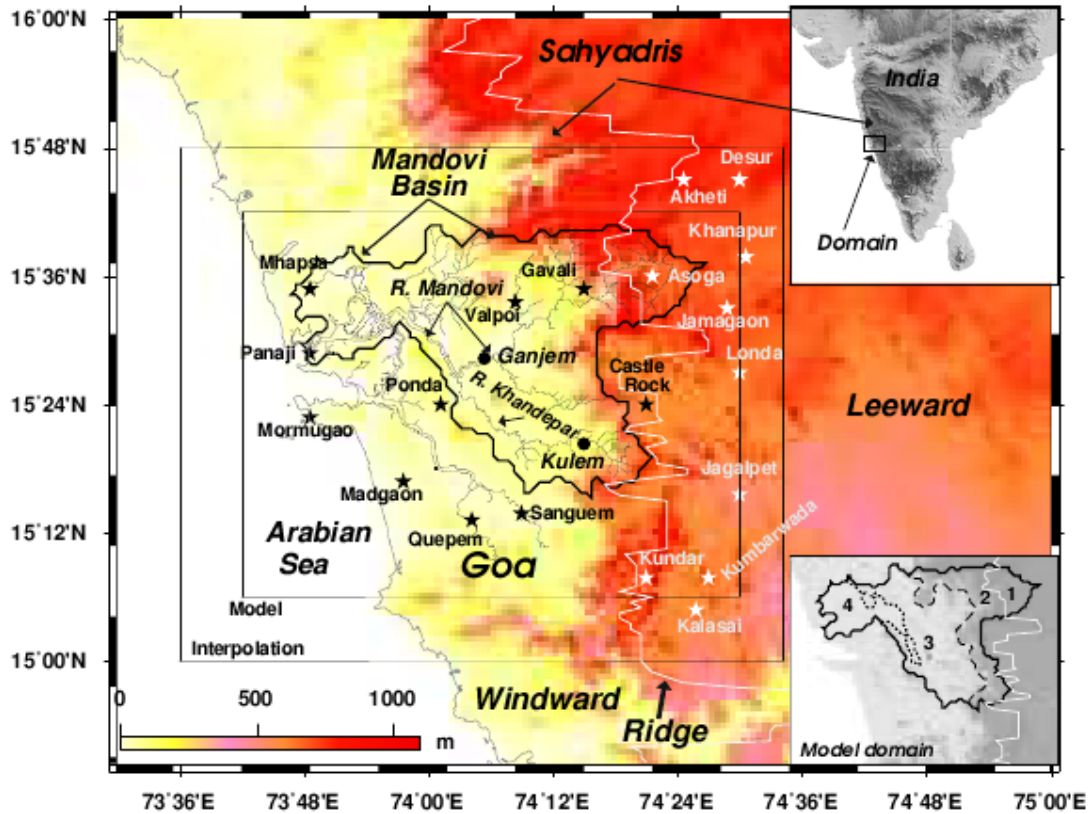


Fig. 1: The topography of the region as in the edited GLOBE DEM. The Mandovi (basin shown by the black curve) originates in the Sahyadris and drains into the Arabian Sea near Panaji. The discharge gauge on the Mandovi is located at Ganjem. The outer and inner rectangles denote the rainfall-mapping and THMB domains. The white jagged line shows the ridge separating the windward (high rainfall) and leeward (low rainfall) sides of the Sahyadris. Stations on the windward (leeward) sides are marked in black (white). The four spatial regions, Lee (1), Ridge (2), Foothills (3), and Coast (4), are shown in lower right inset.

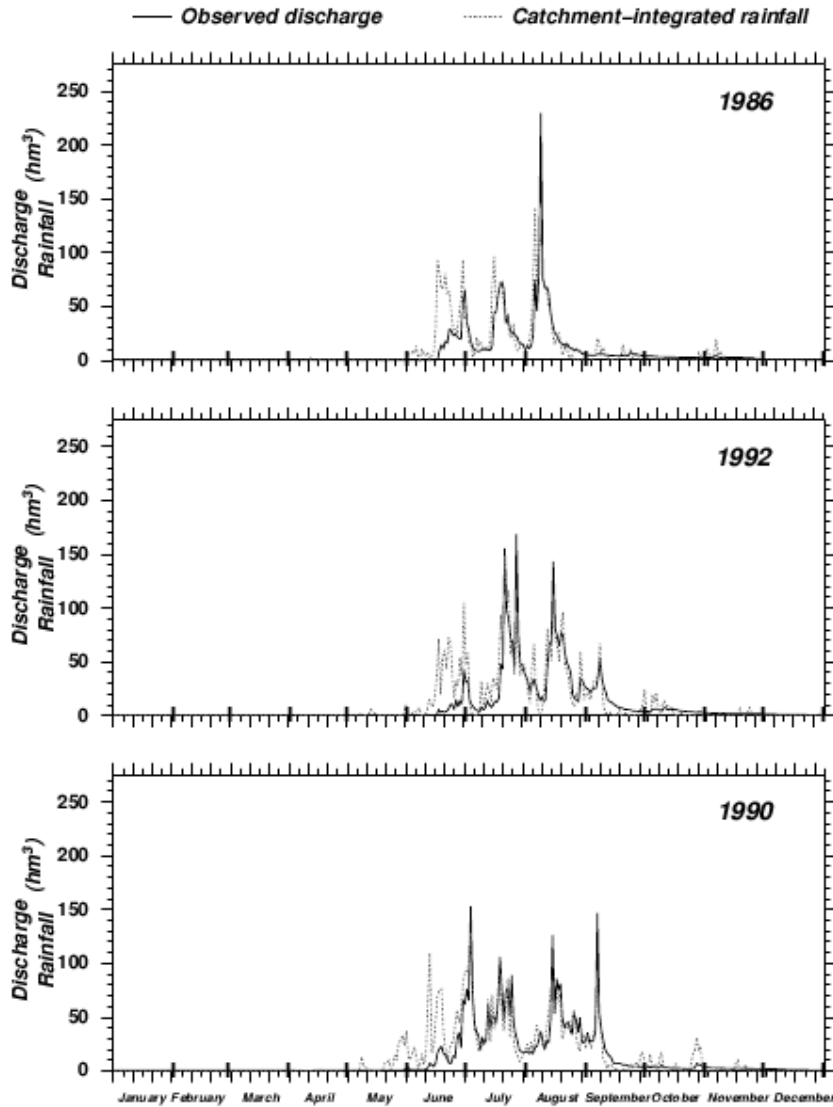


Fig. 2: Daily observed discharge (solid curve, in hm^3/d) at Ganjem and the rainfall integrated over the catchment (dotted curve, in hm^3/d) for 1986 (low-rainfall year, top), 1992 (average-rainfall year, middle), and 1990 (high-rainfall year, bottom). Daily rainfall maps obtained by interpolating the rain gauge data (Fig. 1) were integrated over the catchment area at Ganjem to obtain the “catchment-integrated rainfall”. The bold tick marks on the abscissa indicate beginning and end of a month.

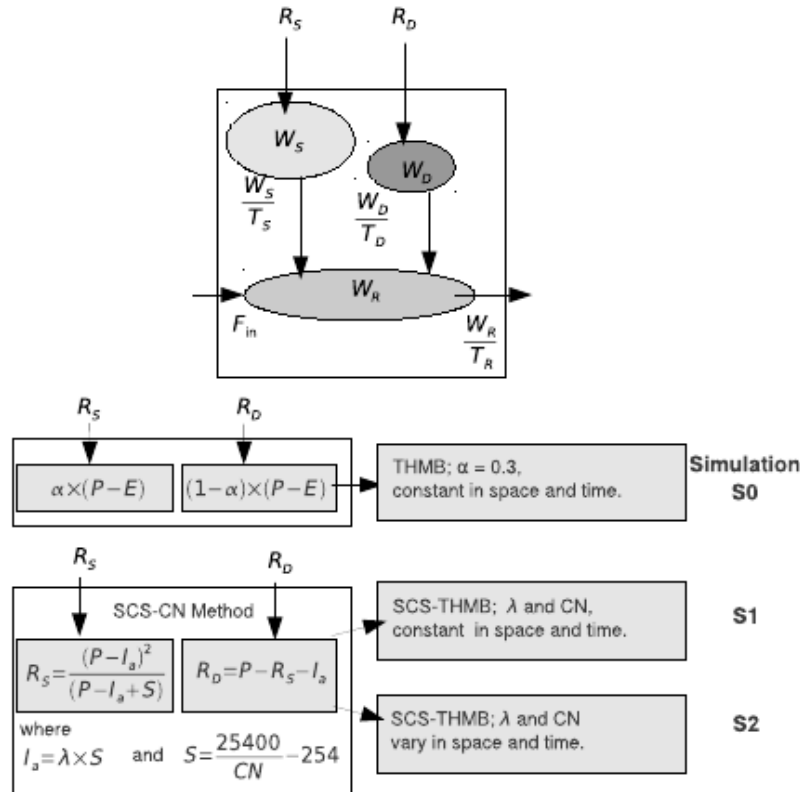


Fig. 3: Schematic representation of THMB (top) with the Soil Conservation Service Curve Number (SCS) method incorporated (bottom) to parametrise the rainfall-runoff relationship. The top panel shows a THMB grid cell, indicated by the dashed line, and the fluxes into and out of the three reservoirs associated with each cell. The surface (subsurface) runoff is R_S (R_D) and it flows into the surface (subsurface) water reservoir W_S (W_D). T_S (T_D) is the time scale over which water flows out of the surface (subsurface) reservoir into the river-water reservoir (W_R), from which water flows out of the cell to a downstream cell over a time scale T_R . $\sum F_{in}$ is the total inflow from all upstream cells into the river-water reservoir. The bottom panel shows how R_S and R_D are parameterised using THMB and the SCS method. Three simulations were done. Simulation S0 used THMB, while S1 and S2 used THMB with the SCS method (SCS-THMB). The difference between S1 and S2 simulations is shown at bottom-right in the figure.

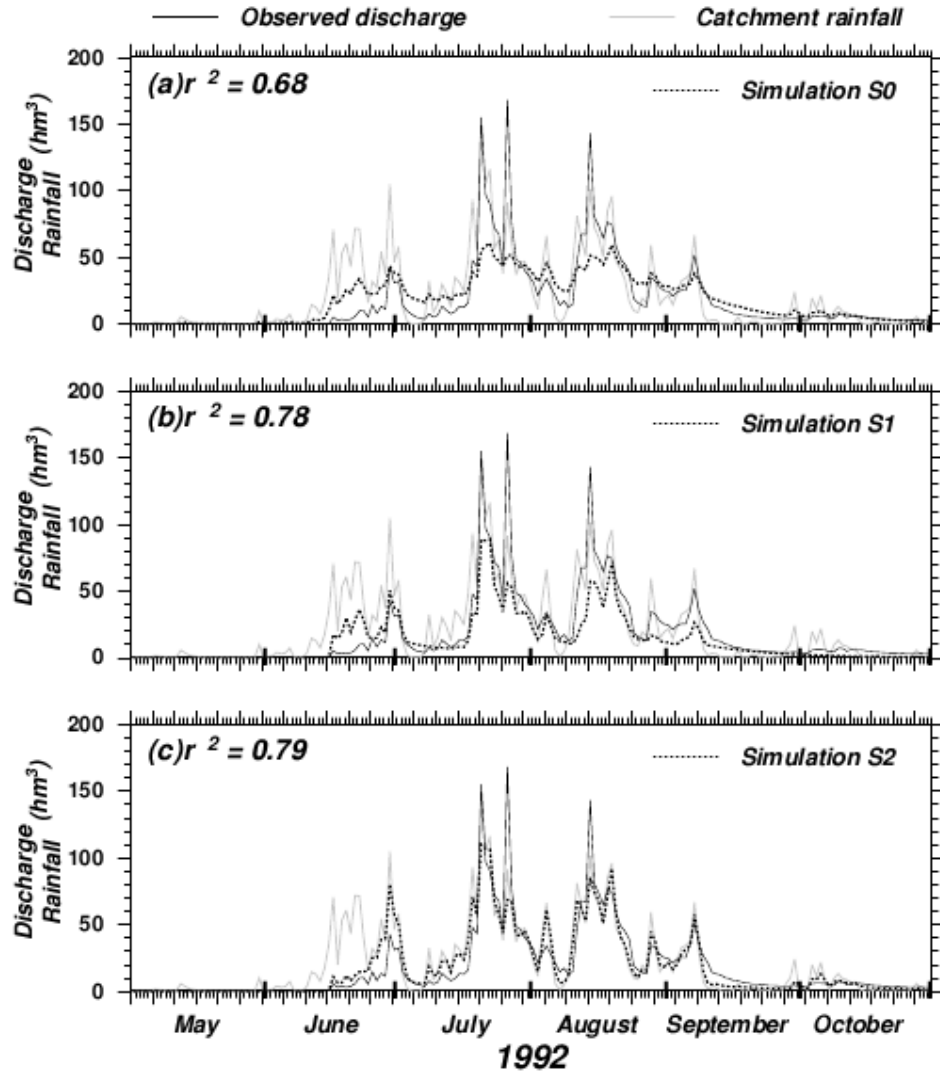


Fig. 4: Daily observed discharge (black), catchment-integrated rainfall (grey), and simulated discharge (dotted) for May–October 1992. The units are hm^3 . (a) Simulation S0. (b) Simulation S1. (c) Simulation S2. Square of the correlation (r^2) between the simulated and observed discharge is computed over the period May–October for the three calibration years (1986, 1990, and 1992). The bold tick marks on the abscissa indicate beginning and end of a month.

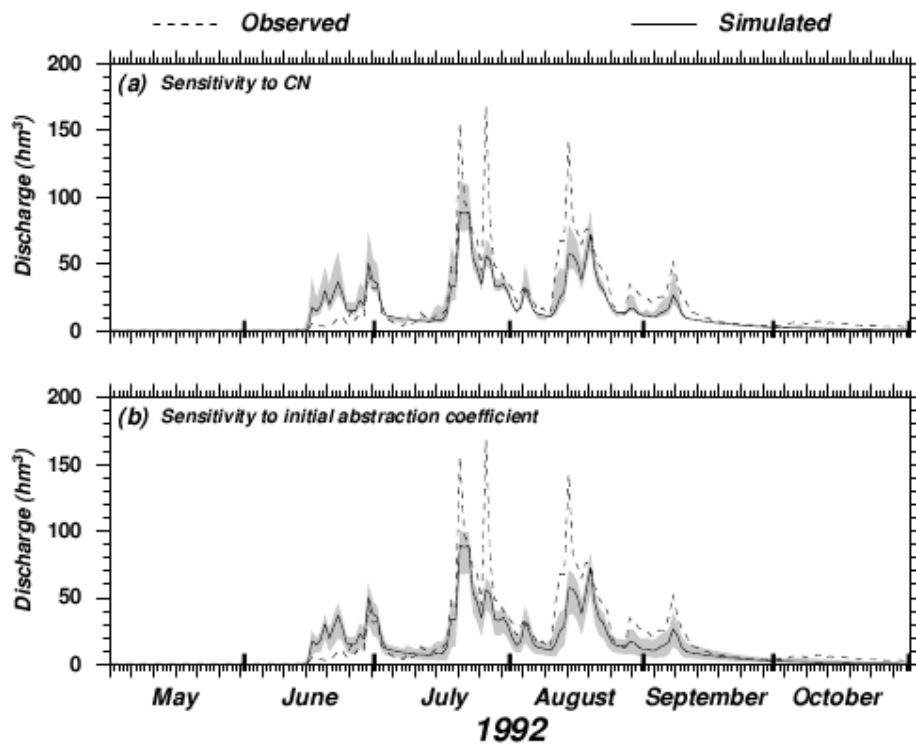


Fig. 5: Sensitivity tests for the SCS parameters. The parameters were constant in space and time, as in Simulation S1. The dashed (solid) curve shows the observed (simulated) discharge and the light grey band shows the range of the simulated discharge over the parameter range in the sensitivity test; the units are hm^3 . (a) Sensitivity to $\text{CN}(\text{II})$. $\text{CN}(\text{II})$ was varied in the range 60–90. The simulated discharge was higher for higher values of $\text{CN}(\text{II})$. (b) Sensitivity to λ , which was varied in the range 0.05–0.6. The simulated discharge was higher for lower values of λ .

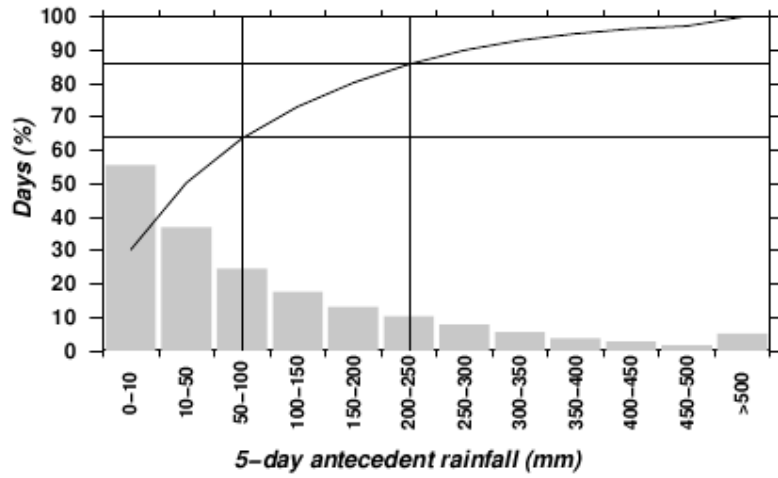


Fig. 6: Determination of the AMC thresholds for Simulation S1. The histogram shows the percentage of the total days (during May–October) that had a five-day antecedent rainfall in the rainfall bands (mm) marked on the abscissa. The histogram was drawn by averaging the number of days in each band over the entire basin and summing over the three years 1986, 1992, and 1990. The curve is the cumulative fraction. The vertical lines represent the lower (100 mm) and upper (250 mm) thresholds.

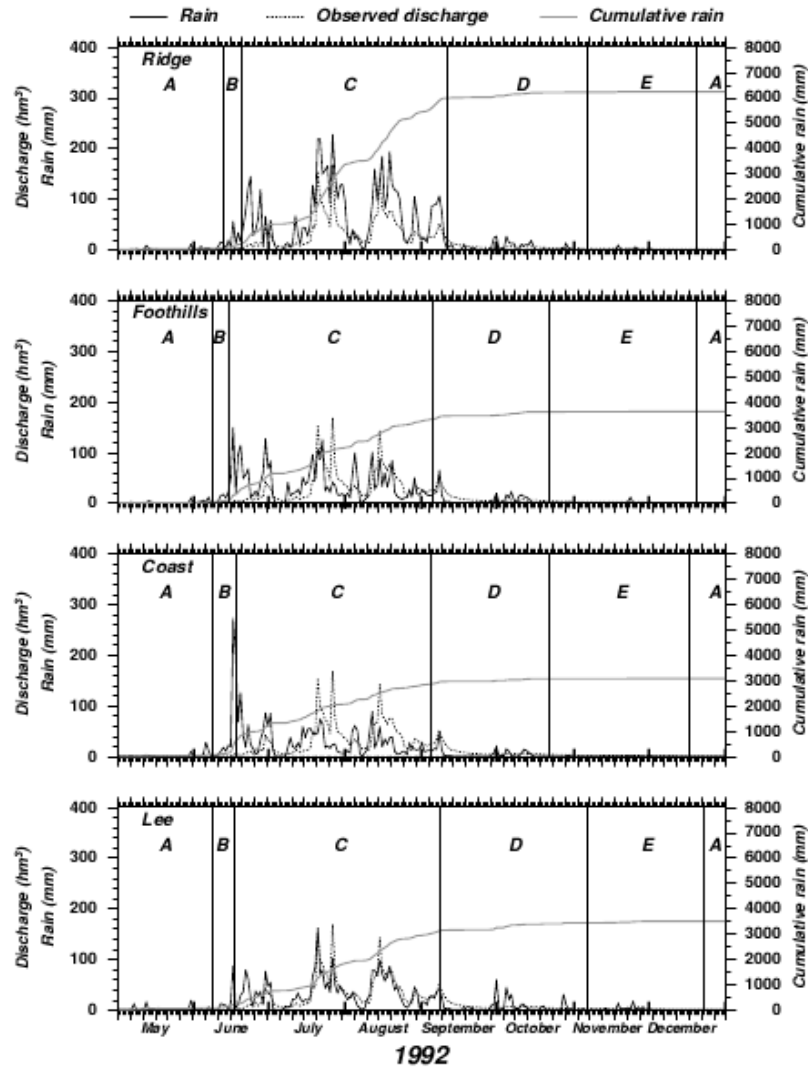


Fig. 7: The temporal regimes, A–E, and the inter-regime transitions for the Ridge, Foothills, Coast, and Lee regions during 1992. The vertical lines mark the transition from one regime to the next. The daily rainfall (solid black curve, in mm) and the cumulative rainfall (CR; solid grey curve, in mm) over one grid cell are shown. The observed discharge (dotted curve, in hm^3) at Ganjem is also plotted.

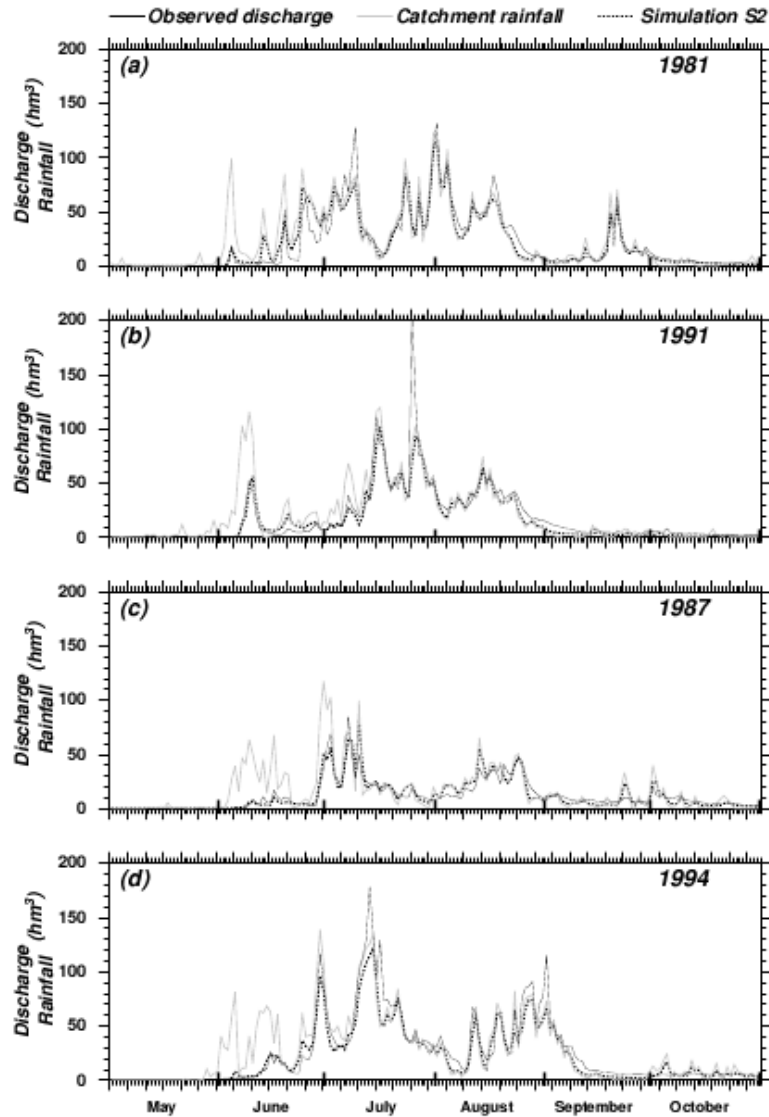


Fig. 8: Observed discharge (black), catchment-integrated rainfall (light grey), and simulated discharge (dotted; Simulation S2) for May–October. The units are hm^3 . (a) 1981. (b) 1991. The daily observed discharge on 26 July 1991 is 207.6 hm^3 , but we have truncated the ordinate to 200 hm^3 . (c) 1987. (d) 1994. 1981 and 1991 are years for which rainfall data are available for all 20 stations; in 1987 and 1994, rainfall data are missing for some stations (see Table III in SS08).

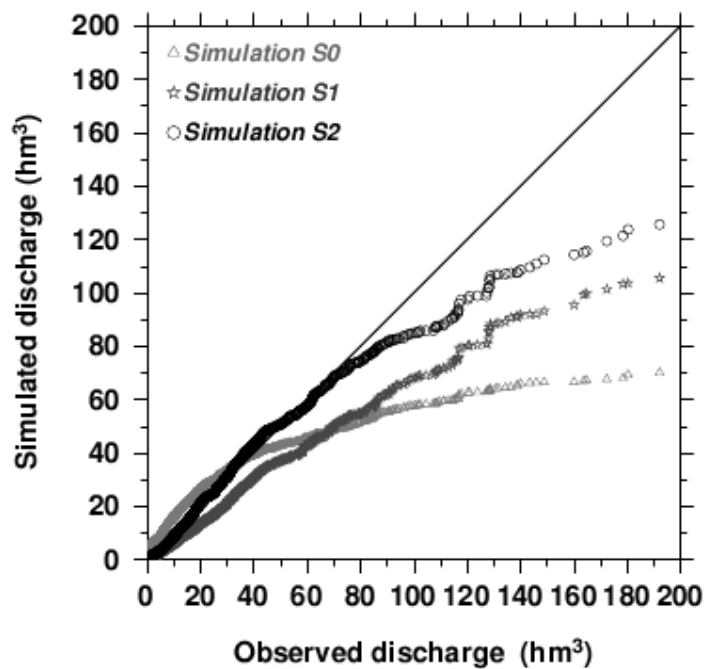


Fig. 9: Correspondence plot between the daily observed discharge (abscissa; hm^3) and simulated discharge (ordinate; hm^3) for June–September for the 15 validation years. Simulation S2 (black hollow circles) performs much better than S1 (grey hollow stars) and S0 (light grey hollow triangles). The maximum daily observed discharge is 406.5 hm^3 , but we have truncated the abscissa to 200 hm^3 (discarding seven data points out of 1830 days). The underestimation seen in the simulations occurs mostly during July–August, and arises owing to the underestimation of peak rainfall events in the basin.

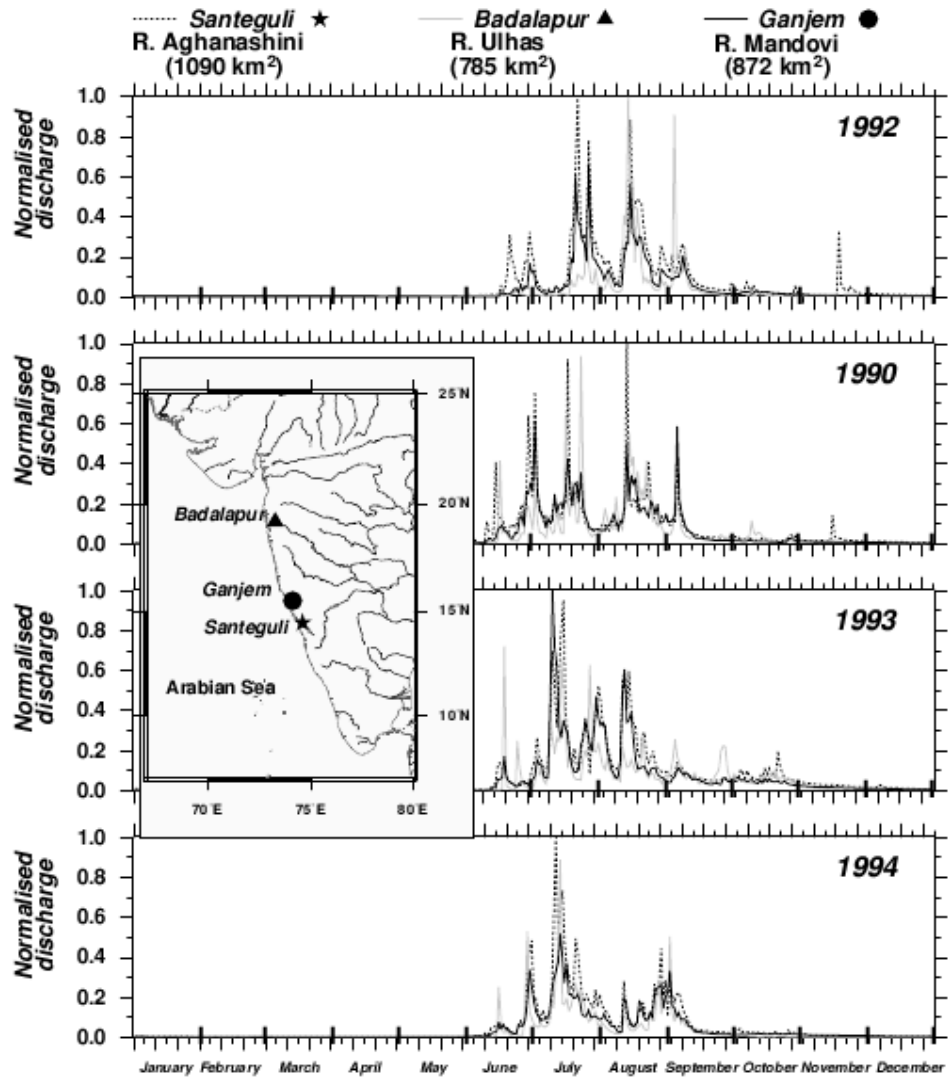


Fig. 10: Daily normalised discharge for three west-coast rivers for 1992, 1990, 1993, and 1994. The discharges are normalised by the highest daily discharge occurring in the particular year. The rivers are Mandovi (black), Aghanashini (dotted), and Ulhas (grey). The catchment area of the Mandovi, Aghanashini and Ulhas are 872 km², 1070 km², 785 km², respectively, at the location of the discharge gauge (gauge locations are marked on the inset map).